Thermal modification of aluminum drinking water treatment residuals for removal of Congo red from water

Qingdong Qin, Zhongshuai Jiang, Yan Xu*

School of Civil Engineering, Southeast University, Nanjing 210096, China. Tel. +86 025 83790757, Fax +86 025 83790757, email: qinqingdong@seu.edu.cn (Q. Qin), 343495129@qq.com (Z. Jiang), xuxucalmm@seu.edu.cn (Y. Xu)

ABSTRACT

Aluminum drinking water treatment residuals (Al-WTRs) were calcined at different temperatures and used for the adsorption of Congo red (CR) from aqueous solution. Scanning electron microscopy (SEM), energy dispersive X-ray spectroscopy (EDX), zeta potential measurement, N_2 gas adsorption-desorption, X-ray diffraction (XRD), Fourier transform infrared spectroscopy (FTIR), and thermogravimetric/differential thermalanalysis (TG/DTA) techniques were utilized to characterize the properties of Al-WTRs. The obtained results revealed that the framework integrity of Al-WTRs was not changed within the range of investigated calcination temperatures, while the surface properties, pore structures and specific surface areas changed significantly. Adsorption kinetic data showed that a rapid initial adsorption rate of Al-WTRs was obtained at calcination temperatures higher than 200 °C. Isothermal adsorptions showed that the optimum calcination temperature for CR adsorption was 400°C and the maximum adsorption capacity was 72.5 mg/g. Compared to other industrial waste solids used as adsorbents, Al-WTRs calcined at 400°C exhibited a relatively higher adsorption capacity for CR. These findings suggested that optimizing the calcination temperature could be an effective approach to increase the adsorption rate and capacity of Al-WTRs for CR removal.

Keywords: Adsorption; Congo red; Drinking water treatment residuals; Thermal modification; Isotherm

1. Introduction

The effluent water of many industries such as textile industries, pulp mills and dyestuff manufacturing, contains large amounts of hazardous dyes, which are of great concern all over the world [1]. Color is the first contaminant to be recognized in wastewater. The presence of low levels of dyes in water (even less than 1 ppm for some dyes) is highly visible and aesthetically unpleasant [2]. Additionally, a variety of dyes or their metabolites are considered as possible carcinogens or mutagens to aquatic life and humans [1,2]. Therefore, it is necessary to remove dye in the wastewater before it is released into the environment.

Various treatment processes such as physical separation, chemical oxidation and biological degradation have been widely employed for the removal of dyes from wastewaters [1,2]. Among the treatment options applied, considerable attentions have been paid to adsorption technology as an efficient and versatile approach. The selection of a suitable adsorbent is crucial for the application of adsorption process. As a commonly used adsorbent, activated carbon has a high capacity for the removal of dyes [2]. However, activated carbon is relatively expensive and difficult to regenerate, which gives the increase in cost of the wastewater treatment. Most recently, many researchers have focused on the naturally available low cost, eco-friendly and effective adsorbents such as industrial by-products, plant waste, fruit waste, fly ash and clay for the removal of dyes [2,3].

*Corresponding author.

Drinking water treatment residuals (WTRs) are non-hazardous byproducts of drinking water treatment produced daily and in large amounts [4,5]. They are produced by the addition of aluminum or iron salts as primary coagulants to raw water to remove colloids, fine soil particles, and natural organic matter. WTRs have a relatively large surface area and are highly reactive, which give them several potential applications as adsorbents for negatively charged ions removal such as phosphate [6], fluoride [7], perchlorate [8], and arsenic [9]. Besides, WTRs have been recycled for soil amendment [10]. The successful applications of WTRs indicate that WTRs are effective and attractive adsorbents in environmental remediation. However, WTRs usually contain a certain amount of organic substances, which can not only occupy the adsorption sites in WTRs, but also form a diffusion-limiting layer on the surface of WTRs [11]. Thus, some pretreatment procedures are necessary to improve WTRs adsorption capacity. Wang et al. demonstrated that phosphorus adsorption capability on ferric and alum WTRs can be enhanced by sequential thermal and acid activation [11]. In addition, they found that oxygen-limited heat treatment significantly increased the adsorption capability of WTRs for heavy metals [12]. However, to the extent of our knowledge, there are few studies on the removal of dyes with WTRs [13]. The influence of the calcination temperature of WTRs to their adsorption ability for dyes from aqueous solution remains unclear.

In the present study, aluminum drinking water treatment residuals (Al-WTRs) are utilized as adsorbents for the removal of Congo red (CR). The effects of calcination temperature on the physical and chemical properties of Al-WTRs as well as the subsequent CR adsorption density of these materials were carefully investigated. The overarching goal of this study is to achieve a better understanding of the changes of Al-WTRs properties with thermal treatment and the influence of corresponding Al-WTRs properties on CR adsorption.

2. Materials and methods

The Al-WTRs were collected from an open air disposal site located next to the Binjiang Drinking Water Treatment Plant in Nanjing, Jiangsu province, China, where aluminum sulfate was employed for Yangtze River surface water flocculation. The Al-WTRs material was air-dried at room temperature for a period of 4 weeks. Then, Al-WTRs were ground to less than 38 μm in diameter and calcined under air atmosphere with a heating rate of 15°C/min to reach five settled gradient temperatures (200, 300, 400, 500 and 600°C) for 4 h. The produced solids were denoted as Al-WTRs-200, Al-WTRs-300, Al-WTRs-400, Al-WTRs-500 and Al-WTRs-600, respectively. The negatively charged dye, CR is the sodium salt of 3,3′-([1,10-biphenyl]-4,4′-diyl) bis (4-aminonaphthalene-1-sulfonic acid) with a formula: $C_{32}H_{22}N_6Na_2O_6S_2$. CR has a molecular weight of 696.66 g/mol and was obtained from Sigma-Aldrich with 99.99% purity. Stock solutions of CR were prepared by dissolving the dye in distilled water.

Powder X-ray diffraction (XRD) patterns of Al-WTRs were recorded on a Bruker D8-Discover diffractometer using Cu $K\alpha$ radiation. N_2 adsorption-desorption isotherms were measured at 77 K on a Micromeritics ASAP 2020 sorptometer, with the samples out gassed for 16 h at 110°C and 10^{-6} Torr prior to measurement. Scanning electron microscopy (SEM) was carried out by FEI 3D apparatus coupled with energy dispersive X-ray spectroscopy (EDX). Fourier transform infrared spectroscopy (FTIR) spectra of Al-WTRs were recorded with KBr pellets on a Perkin-Elmer Spectrum One FTIR between wave numbers of 400 and 4000 cm^{-1}. Thermal analysis of the samples was performed on a Shimadzu DTG-60H Simultaneous DTA-TG apparatus from 20 to 800°C with a heating rate of 12°C/min. Zero point of charge was determined using a ZetaSizer 3000 (Malvern Instrument). The sample containing 0.2 g/L Al-WTRs was suspended in a 0.01 mol/L NaCl solution (electrolyte). Then, the equilibrated slurry was injected into the microelectrophoresis cell using disposable syringes to determine the zeta potential at different pH values. Prior to each measurement, the electrophoresis cell was thoroughly washed and rinsed with deionized water, followed by the introduction of the sample solution to be measured.

Adsorption experiments were performed by batch technique to obtain the adsorption rate and equilibrium data. In brief, the CR adsorption experiments were all conducted in distilled water and room temperature at a constant pH 7.2. For adsorption kinetics, a suspension containing 0.5 g of Al-WTRs were mixed by stirring the mixture at 200 rpm with a 500 mL aqueous solution of CR at a known initial concentration in a flask immersed in a temperature-controlled water bath kept at constant working temperature (24.5°C ± 0.5°C). An aliquot of 2.0 mL of the solution was withdrawn at appropriate time intervals and immediately filtered through a cellulose acetate membrane of 0.45 μm pore size. The residual concentration of CR in the filtrate was subsequently determined by UV-vis spectrophotometer at the wavelength corresponding to the maximum absorbance (λ_{max} = 497 nm). A five-point calibration curve was made with CR standard solutions ranged from 5.0 mg/L to 100 mg/L. To ensure that the adsorption of CR onto the cellulose acetate membrane was negligible, the concentrations of CR standard solutions passed through the filter membrane were measured and recalculated using the calibration curve and the differences were less than 2%. For isotherm studies, a certain amount of adsorbent (0.02 g) was placed in a 50-mL flask, into which 20 mL of CR solution with varying initial concentrations were added. The experiments were performed in a temperature-controlled water bath shaker for 48 h at a mixing speed of 180 rpm. The shaking time was deemed sufficient to ensure apparent equilibrium as determined by preliminary kinetic tests. After the adsorption reached equilibrium, the solutions were filtered and the remaining concentrations of CR were measured by UV-vis spectrophotometer. The samples were diluted if necessary to ensure the CR concentration in the diluted samples were within the range of the calibration curve. The amount of CR adsorbed onto Al-WTRs was calculated from the mass balance equation. To ensure reproducibility, all CR adsorption tests were carried out in duplicate. The coefficients of variations (CV) of the duplicates were all below 5%.

3. Results and discussion

3.1. Characterization of Al-WTRs

SEM images of the Al-WTRs are illustrated in Fig. 1. The Al-WTRs were heterogeneous mixtures of particles with irregular shape and variable size, which showed a lack of crystal structure. The particles of Al-WTRs (raw Al-WTRs, Al-WTRs-200, Al-WTRs-300 and Al-WTRs-400) had fluffy appearance indicating highly porous structure, which was also supported by the specific surface areas measurement.

The changes in the surface elemental composition were monitored by EDX-ray spectroscopy and the results are shown in Table 1. It was observed that chemical composi-tions for Al-WTRs were similar to other Al-WTRs reported elsewhere [8]. The major inorganic components in the Al-WTRs included aluminum, iron and silica. The organic C content decreased with increasing calcination tempera-ture, indicating that some organic components such as humic substances disappeared at high calcination tempera-ture [11].

The N_2 gas adsorption/desorption isotherms were used to determine the pore size, pore volume and sur-face area. The results are shown in Table 1. It was clearly seen that the mesopore volume at pore radius 2–50 nm showed an order of Al-WTRs-300 > Al-WTRs-200 ≈ Al-WTRs-400 ≈ Al-WTRs-500 ≈ Al-WTRs-600 > raw Al-WTRs. These results suggested that calcination sig-nificantly affected the pore structures of Al-WTRs. The specific surface areas of Al-WTRs are also listed in Table 1. It was observed that Al-WTRs-300 had the largest spe-cific surface area. It is likely that water and some impu-rities were expulsed from the Al-WTRs to create more porosity and ultimately enlarge the specific surface area

(a) (b) (c)

(d) (e) (f)
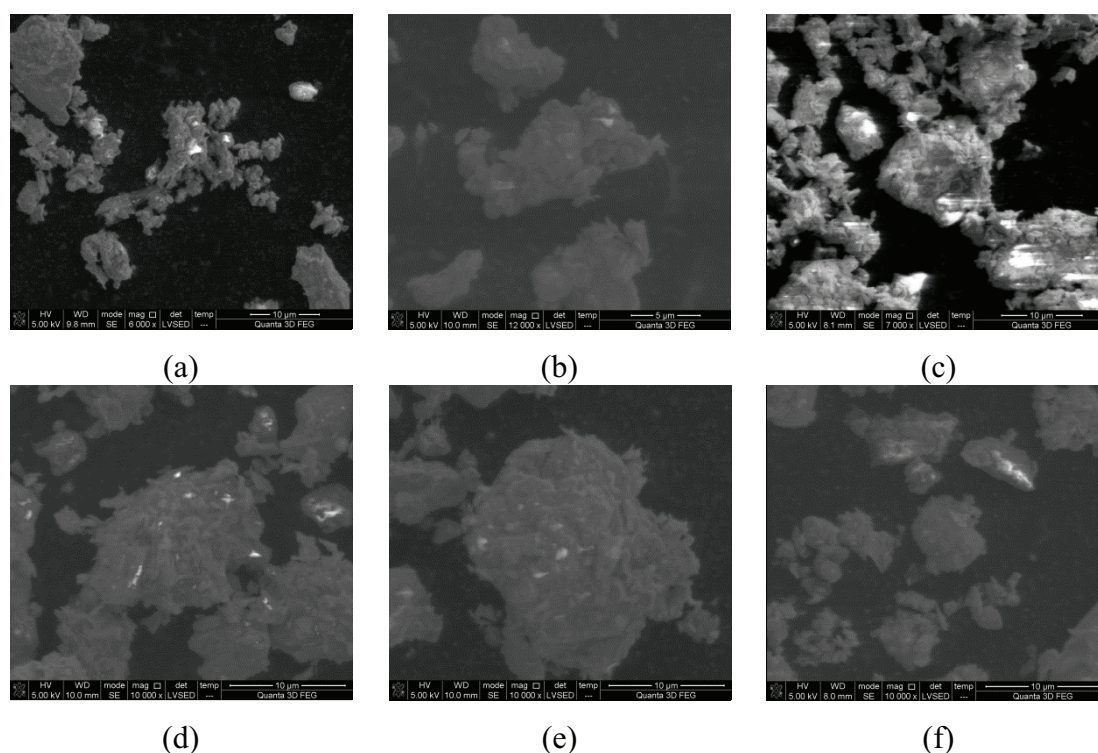
Fig. 1. SEM micrographs of Al-WTRs: (a) Al-WTRs, (b) Al-WTRs-200, (c) Al-WTRs-300, (d) Al-WTRs-400, (e) Al-WTRs-500, and (f) Al-WTRs-600.

Table 1
Chemical composition and physical properties of the Al-WTRs

Adsorbent	C (%)	Aluminum (g/kg)	Iron (g/kg)	Silica (g/kg)	pH$_{pzc}$	S_{BET} (m^2/g)	Mesopore volume (cm^3/g)
Al-WTRs	17.6	40.7	29.2	42.2	5.70	24.7	0.0555
Al-WTRs-200	12.4	49.3	38.5	45.9	5.94	23.9	0.0575
Al-WTRs-300	2.4	63.0	40.9	88.0	6.96	28.0	0.0621
Al-WTRs-400	6.6	58.2	58.5	84.0	7.45	24.4	0.0570
Al-WTRs-500	2.9	69.0	47.3	82.3	7.61	19.9	0.0562
Al-WTRs-600	1.5	92.9	46.2	82.4	7.48	18.2	0.0567

[14]. In contrast, Al-WTRs-600 had the smallest specific surface area. It might be attributed to the fact that some hydroxyl groups were decomposed and the sintering shrinkage of Al-WTRs occurred at 600°C and led to the collapse of pore structure [15,16].

The pH values at the point of zero charge (pH_{pzc}) of Al-WTRs are showed in Table 1. The pH_{PZC} value of the raw Al-WTRs was similar to other aluminum-derived WTRs reported previously [17]. In addition, the raw Al-WTRs were more acidic than the calcined Al-WTRs. This increasing trend of pH_{pzc} along with the increasing calcination temperatures was likely resulted from combustion and/or decomposition of natural organic matter such as humic substances. It was reported that natural organic matter in surface water could be absorbed by aluminum hydroxide precipitates after the flocculation-clarification process during drinking water treatment [12]. The natural organic matter adsorbed in Al-WTRs surface was able to decrease pH_{pzc} of Al-WTRs by its abundant carboxylic acid groups [12].

The XRD patterns of the Al-WTRs are shown in Fig. 2. The XRD pattern of the raw Al-WTRs (Fig. 1(a)) was similar with those reported previously, which displayed that the raw Al-WTRs contained quartz, feldspar and illite/smectite [18]. Additionally, X-ray diffraction analysis revealed that there was no crystalline $Al(OH)_3$ component, indicating that Al-WTRs was amorphous and particles poorly ordered. The peaks remained almost unchanged after calcination, although a decrease in peak 12.5° along with the increasing calcination temperature was noticed, which might be due to the distortion of mesoporous channels caused by the collapse of pore structure during the calcination process [15].

The FTIR spectra of Al-WTRs before and after calcination are shown in Fig. 3. It can be seen that the spectrum of raw Al-WTRs was similar to that of Al-WTRs-200, Al-WTRs-300, and Al-WTRs-400, which indicated that the increase of temperature from 200–400°C did not affect their surface chemical properties apparently. However, the peaks at 3696, 3620, 1430, and 915 cm⁻¹ disappeared after calcination at 500 and 600°C, which suggested the great changes of Al-WTRs surface properties. In the case of raw Al-WTRs, the spectrum exhibited the absorption bands at 3696, 3620,
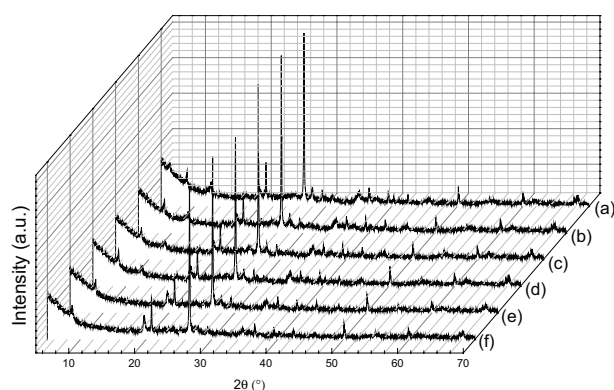
3440, 1640, 1430, 1030, 915, 797, 534 and 463 cm⁻¹. The presence of such bands can be related to the chemical complexity of the Al-WTRs which incorporate organic and inorganic substances. The peaks at 3696 and 3620 cm⁻¹ (present in raw Al-WTRs, Al-WTRs-200, Al-WTRs-300, and Al-WTRs-400) were most likely to correspond to the stretching vibration generated by the hydroxyl groups in Al-WTRs [19,20]. The broadened band around 3440 cm⁻¹ (present in all Al-WTRs) could be assigned to the bending vibration of adsorbed molecular water and/or stretching vibration of hydroxyl group [19]. The peak at 1640 cm⁻¹ (present in all Al-WTRs) belonged to the O–H bending vibration of adsorbed water, which was derived from the interlayer water in Al-WTRs [19]. Apparently, this peak went smaller in the calcined Al-WTRs due to water desorption at high calcination temperature. The observed band at 1430 cm⁻¹ (except Al-WTRs-600) could be assigned to C–H deformation of CH_2 and CH_3 groups [9,20,21]. The sharp peak at 915 cm⁻¹ can be attributed to the vibration of the hydroxyl group combined with Al atoms [20]. It disappeared in Al-WTRs-500 and Al-WTRs-600, demonstrating the surface hydroxyl condensation of Al-WTRs at high calcination temperature. The absorption bands of Al-WTRs appeared at 1030, 797, and 463 cm⁻¹ (present in all Al-WTRs) which were attributed to asymmetric stretching vibration of Si–O–Si, symmetric stretching vibration of Si–O–Si and bending vibration of O–Si–O respectively [22]. The peak at 534 cm⁻¹ was assigned to Si–O–Al (octahedral Al) bending vibrations [22].

Thermogravimetric analyses of Al-WTRs were carried out under flowing air. The TG and DTA profiles corresponding to Al-WTRs samples are depicted in Fig. 4 and exhibited a similar trend. Full temperature range (25–800°C) TG

Fig. 2. XRD patterns of Al-WTRs: (a) Al-WTRs, (b) Al-WTRs-200, (c) Al-WTRs-300, (d) Al-WTRs-400, (e) Al-WTRs-500, and (f) Al-WTRs-600.
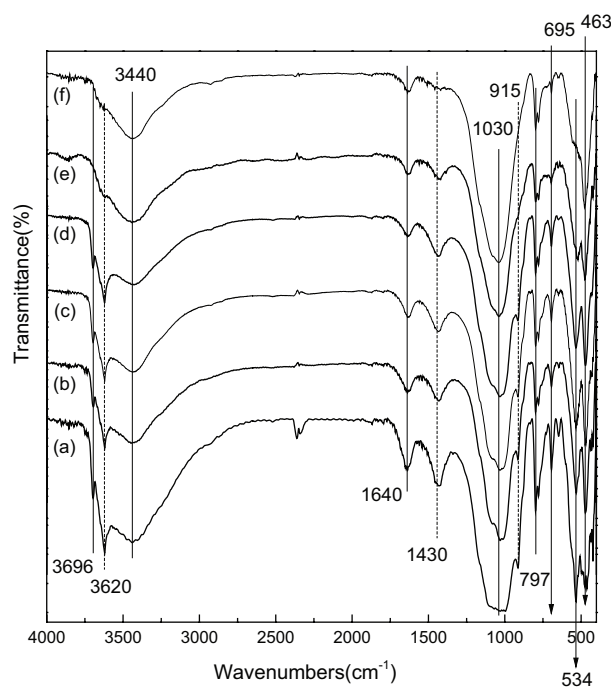
Fig. 3. FTIR spectra of Al-WTRs:(a) Al-WTRs, (b) Al-WTRs-200, (c) Al-WTRs-300, (d) Al-WTRs-400, (e) Al-WTRs-500, and (f) Al-WTRs-600.
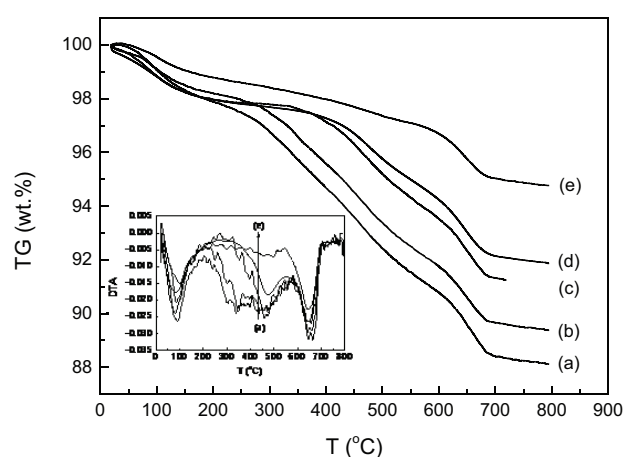
Fig. 4. TG profiles with inset the corresponding DTA curves of Al-WTRs:(a) Al-WTRs, (b) Al-WTRs-200, (c) Al-WTRs-300, (d) Al-WTRs-400, and (e) Al-WTRs-500.

Fig. 5. Effect of contact time on CR adsorption (experimental conditions: pH 7.2; Al-WTRs dose, 1 g/L; Initial CR concentration, 50 mg/L).

analyses for raw Al-WTRs, Al-WTRs-200, Al-WTRs-300, Al-WTRs-400 and Al-WTRs-500 showed a maximum weight loss of about 11.9%, 10.6%, 8.7%, 8.2% and 5.2%, respectively. Most of the weight loss could be attributed to water desorption, organic matter combustion and metal hydroxides dehydroxylation, which was consistent with the weight loss of Fe-WTRs [23].

It was observed from DTA profiles (Fig. 4) that there were three distinct stages in full temperature range (25–800°C) for the raw Al-WTRs. These stages were probably resulted from specific thermal events. The first stage (25–200°C) was usually associated to the release of occluded water. The second stage (200–500°C) was likely caused by the decomposition organic matter combustion, since organic C decomposition weight losses begin at temperatures ≥200°C [23]. The third stage (600–700°C) was derived from the dehydroxylation of metal hydroxides [16]. However, only two stages were found for Al-WTRs-500 in full temperature range (25–800°C). The very limited mass loss in temperature range (200–500°C) for Al-WTRs-500 indicated that most carbonaceous materials had been removed at calcination temperature 500°C. Results given by TG/DTA analysis are in good agreement with that obtained by EDX and FTIR analyses. Similar findings were also reported by Tantawy[24].

3.2. Kinetics of adsorption

The kinetic behavior of the adsorption process was studied under the temperature of 24.5°C ± 0.5°C and pH 7.2. Shown in Fig. 5, for all Al-WTRs, there was a rapid uptake of CR during the initial stage of the adsorption process within the first 1 min, indicating a high affinity between CR molecules and the Al-WTRs surface. Following this phase, the adsorption process slowed down, suggesting a gradual equilibrium, possibly due to the intraparticle diffusion of CR molecules.

Kinetic modeling not only allows estimation of adsorption rates but also provides insights into the possible reaction mechanisms. In this respect, the pseudo-first-order, pseudo-second-order and Elovich equations were used to fit the experimental data [25].
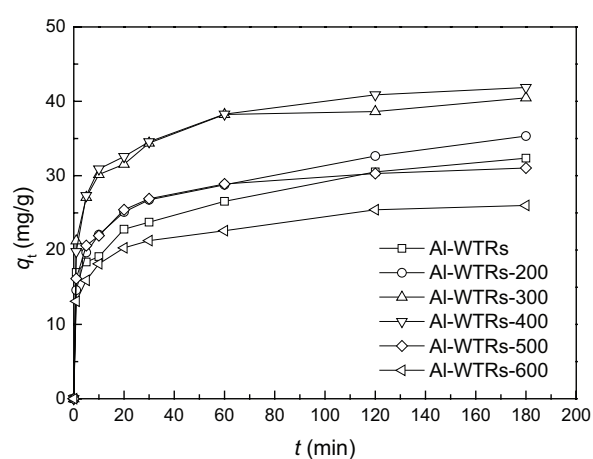
The pseudo-first-order kinetic model is given as follows:

$$q_t = q_e \left(1 - e^{-k_1 t}\right) \tag{1}$$

where q_e and q_t are the amounts of dye adsorbed on adsorbent at equilibrium and at time t (min), respectively (mg/g), and k_1 is the rate constant of pseudo first-order adsorption (min^{-1}).

The pseudo-second-order kinetic model is expressed by the following equation:

$$q_t = \frac{k_2 q_e^2 t}{1 + k_2 q_e t} \tag{2}$$

where k_2 is the rate constant of the pseudo-second-order model (g/mg/min). This model is based on the assumption that the rate-limiting step involves chemisorption of adsorbate on the adsorbent.

The Elovich equation is given as follows:

$$q_t = \frac{\ln(\alpha)}{\beta} + \frac{lnt}{\beta} \tag{3}$$

where α is the initial adsorption rate of Elovich equation (mg/g/min), and the parameter β is related to the extent of surface coverage and activation energy for chemisorptions (g/mg).

In order to quantitatively compare the applicability of different kinetic models in fitting to data, a normalized standard deviation, Δq (%), was calculated as follows:

$$\Delta q(\%) = 100 \times \sqrt{\frac{\sum(q_{texp} - q_{tcal} / q_{texp})^2}{n - 1}} \tag{4}$$

where n is the number of data points; q_{texp} is the experimental values; and q_{tcal} is the calculated values by the model.

The results from fitting experimental data with pseudo-first and pseudo-second-order models and Elovich

Table 2
Parameters of kinetic model of CR adsorption onto Al-WTRs

Adsrobent	Pseudo-first-order model			Pseudo-second-order model			Elovich		
	k_1 (min^{-1})	q_e (mg/g)	Δq (%)	k_2 (g/mg/min)	q_e (mg/g)	Δq (%)	α (mg/g/min)	β (g/mg)	Δq (%)
Al-WTRs	1.10	24.8	21.1	0.032	26.9	18.6	298.6	0.32	8.7
Al-WTRs-200	0.27	28.9	24.3	0.014	30.9	16.6	127.0	0.25	3.4
Al-WTRs-300	0.88	34.5	14.2	0.025	36.8	10.6	1044.8	0.27	2.2
Al-WTRs-400	0.66	35.6	15.1	0.019	38.3	10.8	485.4	0.23	1.7
Al-WTRs-500	0.85	26.6	15.4	0.030	28.5	11.6	608.0	0.33	2.4
Al-WTRs-600	0.83	21.5	17.2	0.033	23.2	13.3	321.7	0.39	2.8

equation are presented in Table 2. It was observed that the order of Δq was pseudo-first > pseudo-second > Elovich model, suggesting the Elovich model was the best to represent adsorption kinetic of CR on Al-WTRs. This result revealed that adsorption of CR on Al-WTRs was mainly controlled by the chemisorption behavior likely attributed to exchanging or sharing of electrons between anionic dyes and Al-WTRs [26]. On the other hand, the α value of raw Al-WTRs was smaller than that of Al-WTRs calcined at 300, 400, 500 and 600°C, indicating that organic substances in raw Al-WTRs could form a diffusion-limiting layer on the surface of Al-WTRs. Moreover, the largest α value was observed in Al-WTRs-300, demonstrating that calcination at 300°C favored a rapid adsorption. Previous studies have confirmed that increasing numbers of mesopores can accelerate the pore diffusion of organic molecules [27]. Therefore, the observed rapid adsorption at 300°C was likely linked to its largest mesopore volume among all studies Al-WTRs (Table 1).

3.3. Adsorption isotherm

To compare adsorption density of Al-WTRs under different calcination temperatures, the adsorption isotherms were assessed. Fig. 6 displays the adsorption isotherms at 24.5°C ± 0.5°C, pH 7.2 of CR on Al-WTRs with a solid/liquid ratio of 1 g/L.

The adsorption of CR onto Al-WTRs exhibited a typical Langmuir-type isotherm (Fig. 6). Therefore, the obtained experimental equilibrium adsorption data were then fitted using Langmuir model:

$$\frac{C_e}{q_e} = \frac{1}{Q_0 K_L} + \frac{C_e}{Q_0} \tag{5}$$

where q_e (mg/g) is the adsorbed amount of CR; C_e (mg/L) is the equilibrium concentration of CR in solution; Q_0 (mg/g) is the maximum mono layer adsorption capacity; K_L (L/mg) is the constant related to the free energy of adsorption. The corresponding parameters are shown in Table 3. It is apparent that the fits are quite well for CR within the concentration range studied (correlation coefficient, $R^2 > 0.99$), suggesting that the adsorption of CR onto Al-WTRs closely followed a Langmuir isotherm. The good fitness with the Langmuir model also suggested that the adsorption was limited by mono layer coverage and the surface was rela-
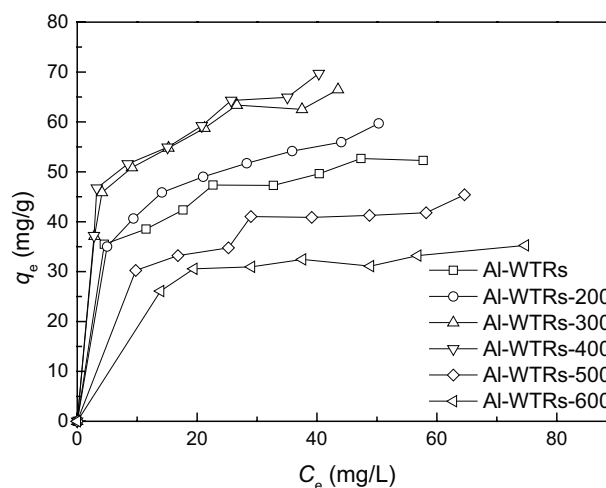
Fig. 6. Adsorption isotherms of CR on Al-WTRs (experimental conditions: pH 7.2; Al-WTRs dose, 1 g/L).

Table 3
Langmuir isotherm constants for CR adsorption onto Al-WTRs

Adsorbent	Langmuir model		
	Q_0 (mg/g)	K_L (L/mg)	R^2
Al-WTRs	56.2	0.22	0.996
Al-WTRs-200	63.7	0.18	0.995
Al-WTRs-300	69.0	0.34	0.997
Al-WTRs-400	72.5	0.31	0.993
Al-WTRs-500	48.5	0.13	0.990
Al-WTRs-600	37.3	0.17	0.995

tively homogeneous. The mono layer saturation capacities (Q_0) of Al-WTRs, Al-WTRs-200, Al-WTRs-300, Al-WTRs-400, Al-WTRs-500 and Al-WTRs-600 were found to be 56.2, 63.7, 69.0, 72.5, 48.5 and 37.3 mg/g, respectively. Q_0 decreased in the following order: Al-WTRs-400 > Al-WTRs-300 > Al-WTRs-200 > Al-WTRs > Al-WTRs-500 > Al-WTRs-600. The adsorption capacity of Al-WTRs-400 was significantly higher than that of raw Al-WTRs. However, the adsorp-

tion capacity of Al-WTRs-600 was much lower than that of other Al-WTRs. On the other hand, the affinity (K_L) of Al-WTRs-400 toward CR molecules was greater than that of raw Al-WTRs, indicating that CR has a stronger adsorption affinity with Al-WTRs-400 surface than that with raw Al-WTRs surface.

In the aqueous solution, CR molecules are dissociated to anionic dye ions at natural solution pH of 7.2. The oxides of Al, Fe and Si present in the Al-WTRs develop charges in contact with water. Except silica, all other oxides possess positive charges under the studied pH as zero point charge of SiO_2, Al_2O_3 and Fe_2O_3 are 2.3, 8.6 and 7.5, respectively [28]. It was proposed that anionic dye adsorption by inorganic solid wastes was favored at pH < pH_{pzc} where a significantly high electrostatic attraction existed between the positively charged surface of the adsorbent and the anionic dye [1,29]. CR is a negatively charged dye and the surface of raw Al-WTRs under experiment pH 7.2 was also negatively charged (pH_{pzc} = 5.70). Therefore, the smaller adsorption capacity of raw Al-WTRs compared to that of Al-WTRs-300 and Al-WTRs-400 was most likely due to the electrostatic repulsion between CR and negatively charged particles. Moreover, the high content of organic substances in the raw Al-WTRs could occupy the adsorption sites [11], resulting in a decrease of CR adsorption. However, significant adsorption of CR by raw Al-WTRs was also observed. This suggested that other interactions might involve in CR adsorption. Fu and Viraraghavan reported that two primary amines (–NH_2)attached to the two naphthalene rings located at the two ends of the CR molecule can be protonated (–NH_3^+) at the initial pH of 6.0 and exhibit stronger basicity, which could result in the attraction between the protonated amine (–NH_3^+)and the negatively charged surface of the adsorbent [30]. It should be noted that the adsorption capacities of Al-WTRs-500 and Al-WTRs-600 were lower than that of Al-WTRs-400, although their zeta potential values were similar. This might be due to the decrease of specific surface area at higher calcination temperatures, where the available adsorption sites were reduced. Nevertheless, it can be concluded that optimizing the calcination temperature can be an accessible approach to achieve a most suitable pH_{pzc} and specific surface area, and finally, maximize the adsorption capacity of Al-WTRs for CR removal.

To compare our data with previous studies, the maximum adsorption capacity (Q_0) of CR on adsorbents based on industrial solid wastes is summarized in Table 4. Comparative values of Q_0 clearly suggested that the adsorption capacity of Al-WTRs-400 was much higher than that of most of industrial by-products such as metal hydroxide sludge, fly ash and red mud. Although electrocoagulated metals hydroxide sludge (EMHS) exhibited a better adsorption capacity than our Al-WTRs-400, the application of EMHS as a CR adsorbent should be carefully assessed because EMHS usually contains a relatively high level of toxic heavy metal Cr, which is possibly introduced to the environment and causes other serious problems [31]. The relatively higher adsorption capacity of acid mine drainage sludge is likely attributed to the chemical precipitation between calcium ion and dye molecules, since calcium ion leaches from the adsorbent material [32,33]. Generally, the present results imply that Al-WTRs can serve as a potential adsorbent for the removal of CR from water.

Table 4
Comparison of the maximum adsorption capacity (Q_0) of adsorbents based on industrial solid wastes

Adsorbent	pH	Q_0 (mg/g)	Reference
Waste red mud	7.3	4.1	[34]
Acid activated red mud	7.0	7.1	[35]
Waste Fe(III)/Cr(III) hydroxide	3.0	44.0	[36]
Metal hydroxides sludge	6.0	40	[37]
Electrocoagulated metals hydroxide sludge	7.0	292.9	[31]
Acid mine drainage sludge	8.1	389.1	[33]
Fly ash	7.5	4.1	[38]
Bagasse fly ash	7.0	11.9	[39]
Calcium-rich fly ash	5.0	12.0	[40]
Pyrolusite reductive leaching residue	~6.0	45.7	[41]
Al-WTRs-400	7.2	72.5	This work

4. Conclusions

Thermal modification of aluminum drinking water treatment residuals for removal of Congo red from water was investigated using the batch adsorption technique. Kinetic data was best interpreted by an Elovich kinetic model. The rapid initial adsorption rate of Al-WTRs calcined at temperatures higher than 200°C was observed, indicating the destruction of diffusion-limiting layer on the surface of Al-WTRs by the organic substances. The adsorption isotherms showed that the highest adsorption capacity was found at calcination temperature of 400°C. These phenomena were successfully linked to the changes of surface properties, pore structures and specific surface areas of Al-WTRs, where the chemical and physical characterization of Al-WTRs revealed that a suitable zeta potential, pore structure and specific surface area of Al-WTRs for CR adsorption were obtained at calcination temperature of 400°C. These findings suggest that optimizing the calcination temperature could be used to increase the adsorption rate and capacity of Al-WTRs for CR removal. Compared to other commonly used industrial waste materials, Al-WTRs-400 showed a relatively higher adsorption capacity for CR. The present results suggest that Al-WTRs have a potential and promising application in the removal of CR from water.

References

[1] M.T. Yagub, T.K. Sen, S. Afroze, H.M. Ang, Dye and its removal from aqueous solution by adsorption: a review, Adv. Colloid Interface Sci., 209 (2014) 172–184.

[2] P. Sharma, H. Kaur, M. Sharma, V. Sahore, A review on applicability of naturally available adsorbents for the removal of hazardous dyes from aqueous waste, Environ. Monit. Assess., 183 (2011) 151–195.

[3] C. Smaranda, M. Gavrilescu, D. Bulgariu, Studies on sorption of congo red from aqueous solution onto soil, Int. J. Environ. Res., 5 (2011) 177–188.

[4] J.A. Ippolito, K.A. Barbarick, H.A. Elliott, Drinking water treatment residuals: a review of recent uses, J. Environ. Qual., 40 (2011) 1–12.

[5] A.O. Babatunde, Y.Q. Zhao, Constructive approaches toward water treatment works sludge management: an international review of beneficial reuses, Crit. Rev. Environ. Sci. Technol., 37 (2007) 129–164.

[6] L.L. Bai, C.H. Wang, Y.S. Pei, J.B. Zhao, Reuse of drinking water treatment residuals in a continuous stirred tank reactor for phosphate removal from urban wastewater, Environ. Technol., 35 (2014) 2752–2759.

[7] S. Vinitnantharat, S. Kositchaiyong, S. Chiarakorn, Removal of fluoride in aqueous solution by adsorption on acid activated water treatment sludge, Appl. Surf. Sci., 256 (2010) 5458–5462.

[8] K.C. Makris, D. Sarkar, R. Datta, Aluminum-based drinking-water treatment residuals: a novel sorbent for perchlorate removal, Environ. Pollut., 140 (2006) 9–12.

[9] P. Castaldi, E. Mele, M. Silvetti, G. Garau, S. Deiana, Water treatment residues as accumulators of oxoanions in soil. Sorption of arsenate and phosphate anions from an aqueous solution, J. Hazard. Mater., 264 (2014) 144–152.

[10] K.B. Dassanayake, G.Y. Jayasinghe, A. Surapaneni, C. Hetherington, A review on alum sludge reuse with special reference to agricultural applications and future challenges, Waste Manage., 38 (2015) 321–335.

[11] C.H. Wang, S.J. Gao, T.X. Wang, B.H. Tian, Y.S. Pei, Effectiveness of sequential thermal and acid activation on phosphorus removal by ferric and alum water treatment residuals, Chem. Eng. J., 172 (2011) 885–891.

[12] C.H. Wang, H.L. Jiang, N.N. Yuan, Y.S. Pei, Z.S. Yan, Tuning the adsorptive properties of drinking water treatment residue via oxygen-limited heat treatment for environmental recycle, Chem. Eng. J., 284 (2016) 571–581.

[13] W. Chu, Dye removal from textile dye wastewater using recycled alum sludge, Water Res., 35 (2001) 3147–3152.

[14] M. Toor, B. Jin, Adsorption characteristics, isotherm, kinetics, and diffusion of modified natural bentonite for removing diazo dye, Chem. Eng. J., 187 (2012) 79–88.

[15] Y.Z. Li, C.J. Liu, Z.K. Luan, X.J. Peng, C.L. Zhu, Z.Y. Chen, Z.G. Zhang, J.H. Fan, Z.P. Jia, Phosphate removal from aqueous solutions using raw and activated red mud and fly ash, J. Hazard. Mater., 137 (2006) 374–383.

[16] Y. Sarikaya, I. Sevinc, M. Akinc, The effect of calcination temperature on some of the adsorptive properties of fine alumina powders obtained by emulsion evaporation technique, Powder Technol., 116 (2001) 109–114.

[17] Y.F. Zhou, R.J. Haynes, Removal of Pb(II), Cr(III) and Cr(VI) from aqueous solutions using alum-derived water treatment sludge, Water Air Soil Pollut., 215 (2011) 631–643.

[18] J.A. Ippolito, K.G. Scheckel, K.A. Barbarick, Selenium adsorption to aluminum-based water treatment residuals, J. Colloid Interface Sci., 338 (2009) 48–55.

[19] N.H. Rodriguez, S.M. Ramirez, M.T.B. Varela, M. Guillem, J. Puig, E. Larrotcha, J. Flores, Re-use of drinking water treatment plant (DWTP) sludge: characterization and technological behaviour of cement mortars with atomized sludge additions, Cem. Concr. Res., 40 (2010) 778–786.

[20] R.A.V. Rossel, T. Behrens, Using data mining to model and interpret soil diffuse reflectance spectra, Geoderma, 158 (2010) 46–54.

[21] P. Castaldi, M. Silvetti, G. Garau, D. Demurtas, S. Deiana, Copper(II) and lead(II) removal from aqueous solution by water treatment residues, J. Hazard. Mater., 283 (2015) 140–147.

[22] J. Madejova, FTIR techniques in clay mineral studies, Vib. Spectrosc., 31 (2003) 1–10.

[23] K.C. Makris, W.G. Harris, Time dependency and irreversibility of water desorption by drinking-water treatment residuals: implications for sorption mechanisms, J. Colloid Interface Sci., 294 (2006) 151–154.

[24] M.A. Tantawy, Characterization and pozzolanic properties of calcined alum sludge, Mater. Res. Bull., 61 (2015) 415–421.

[25] W. Plazinski, W. Rudzinski, A. Plazinska, Theoretical models of sorption kinetics including a surface reaction mechanism: a review, Adv. Colloid Interface Sci., 152 (2009) 2–13.

[26] V. Vimonses, S.M. Lei, B. Jin, C.W.K. Chowd, C. Saint, Kinetic study and equilibrium isotherm analysis of Congo Red adsorption by clay materials, Chem. Eng. J., 148 (2009) 354–364.

[27] C.T. Hsieh, H.S. Teng, Influence of mesopore volume and adsorbate size on adsorption capacities of activated carbons in aqueous solutions, Carbon, 38 (2000) 863–869.

[28] M. Kosmulski, pH-dependent surface charging and points of zero charge III. Update, J. Colloid Interface Sci., 298 (2006) 730–741.

[29] E. Bulut, M. Ozacar, I.A. Sengil, Equilibrium and kinetic data and process design for adsorption of Congo Red onto bentonite, J. Hazard. Mater., 154 (2008) 613–622.

[30] Y.Z. Fu, T. Viraraghavan, Dye biosorption sites in Aspergillus niger, Bioresour. Technol., 82 (2002) 139–145.

[31] A.K. Golder, A.N. Samanta, S. Ray, Anionic reactive dye removal from aqueous solution using a new adsorbent –sludge generated in removal of heavy metal by electrocoagulation, Chem. Eng. J., 122 (2006) 107–115.

[32] V. Vimonses, B. Jin, C.W.K. Chow, Insight into removal kinetic and mechanisms of anionic dye by calcined clay materials and lime, J. Hazard. Mater., 177 (2010) 420–427.

[33] X.C. Wei, R.C. Viadero, Adsorption and precoat filtration studies of synthetic dye removal by acid mine drainage sludge, J. Environ. Eng.-ASCE 133 (2007) 633–640.

[34] C. Namasivayam, D. Arasi, Removal of congo red from wastewater by adsorption onto waste red mud, Chemosphere, 34 (1997) 401–417.

[35] A. Tor, Y. Cengeloglu, Removal of congo red from aqueous solution by adsorption onto acid activated red mud, J. Hazard. Mater., 138 (2006) 409–415.

[36] C. Namasivayam, R. Jeyakumar, R.T. Yamuna, Dye removal from waste-water by adsorption on waste Fe(III)/Cr(III) hydroxide, Waste Manage., 14 (1994) 643–648.

[37] M.F. Attallah, I.M. Ahmed, M.M. Hamed, Treatment of industrial wastewater containing Congo Red and Naphthol Green B using low-cost adsorbent, Environ. Sci. Pollut. Res., 20 (2013) 1106–1116.

[38] V.V.B. Rao, S.R.M. Rao, Adsorption studies on treatment of textile dyeing industrial effluent by flyash, Chem. Eng. J., 116 (2006) 77–84.

[39] I.D. Mall, V.C. Srivastava, N.K. Agarwal, I.M. Mishra, Removal of congo red from aqueous solution by bagasse fly ash and activated carbon: kinetic study and equilibrium isotherm analyses, Chemosphere, 61 (2005) 492–501.

[40] B. Acemioglu, Adsorption of Congo red from aqueous solution onto calcium-rich fly ash, J. Colloid Interface Sci., 274 (2004) 371–379.

[41] W. Shen, B. Liao, W.Y. Sun, S.J. Su, S.L. Ding, Adsorption of Congo red from aqueous solution onto pyrolusite reductive leaching residue, Desal. Water Treat., 52 (2014) 3564–3571.